ARTICLE

X–ray structures and mechanism of the human serotonin transporter

Jonathan A. Coleman[1], Evan M. Green[1]† & Eric Gouaux[1,2]

The serotonin transporter (SERT) terminates serotonergic signalling through the sodium– and chloride–dependent reuptake of neurotransmitter into presynaptic neurons. SERT is a target for antidepressant and psychostimulant drugs, which block reuptake and prolong neurotransmitter signalling. Here we report X–ray crystallographic structures of human SERT at 3.15 Å resolution bound to the antidepressants (*S*)–citalopram or paroxetine. Antidepressants lock SERT in an outward–open conformation by lodging in the central binding site, located between transmembrane helices 1, 3, 6, 8 and 10, directly blocking serotonin binding. We further identify the location of an allosteric site in the complex as residing at the periphery of the extracellular vestibule, interposed between extracellular loops 4 and 6 and transmembrane helices 1, 6, 10 and 11. Occupancy of the allosteric site sterically hinders ligand unbinding from the central site, providing an explanation for the action of (*S*)–citalopram as an allosteric ligand. These structures define the mechanism of antidepressant action in SERT, and provide blueprints for future drug design.

Serotonin (5-hydroxytryptamine or 5-HT) modulates the activity of the central nervous system as well as processes throughout the body ranging from cardiovascular function to digestion, body temperature, endocrinology and reproduction[1]. Discovered in the late 1940s as a signalling molecule, serotonin increases vasoconstriction after blood clotting, that is, serum-tone[2]. In the brain, the raphe nuclei synthesize serotonin from tryptophan, and distribute serotonin via long projections that reach nearly every major brain region. Serotonin is released into the synaptic cleft between neurons, where it diffuses to activate serotonin receptors, a group of G-protein-coupled receptors and ligand-gated ion channels that participate in both excitatory and inhibitory neurotransmission and modulate the release of many neurotransmitters and hormones. Thus, serotonergic signalling influences neurological processes including sleep, mood, cognition, pain, hunger and aggression behaviours. The discovery that serotonin reuptake into nerve terminals is inhibited by the tricyclic antidepressant imipramine in a manner similar to norepinephrine (also known as noradrenaline) reuptake provided an initial clue that transport occurs by a related reuptake system[3–5]. Prozac was introduced as one of the first selective serotonin reuptake inhibitors (SSRIs) for the treatment of depression and, subsequently, the serotonin transporter gene (*SERT*, also known as *SLC6A4*) was cloned and proven to be the target of SSRIs[6,7].

SERT is a member of the neurotransmitter sodium symporter (NSS) family of transporters, which also includes the dopamine (DAT) and norepinephrine (NET) transporters. NSSs are responsible for the sodium- and chloride-dependent reuptake of neurotransmitters, thus terminating signalling of the biogenic amines[8,9]. The unbinding of inhibitors can be further modulated by serotonin[10] and antidepressants[11] acting at an allosteric site. Several neurological conditions are associated with NSS dysregulation, including depression, anxiety disorder, attention-deficit hyperactivity disorder, epilepsy and Parkinson's disease[8,9,12]. Pharmacological modulation of NSS function through the use of therapeutic drugs such as tricyclic antidepressants and SSRIs has been used to treat many psychiatric disorders[13]. Illicit drugs such as cocaine and methamphetamines block neurotransmitter reuptake and are commonly abused psychostimulants, diminishing the well-being of users and constituting a tremendous socioeconomic burden.

Knowledge of NSS structure has been guided, in part, by experiments on the bacterial orthologue LeuT, as well as by studies of the *Drosophila* DAT (dDAT). This previous work has shown that the NSS family of transporters contain an inverted-topological repeat of transmembrane helices (TM) 1–5 and TM6–TM10, a 'central' or primary binding site for substrate and ions approximately halfway across the membrane-spanning region of the transporters[14–18] and, in the outward-open conformation, a large extracellular vestibule. Recently, structures of the invertebrate dDAT have provided insight into NSS pharmacology[19–21]. Nevertheless, these studies fall short of defining the structural determinants responsible for the markedly diverse pharmacological profiles of NSSs, the allosteric mechanism of human SERT, and important characteristics of human transporters. Here we present structures of the human serotonin transporter in complex with two of the most widely prescribed antidepressants: (*S*)-citalopram and paroxetine. Structures of SERT illuminate the molecular features of SSRI inhibition and allosteric regulation, as well as structural elements not reported in transporters previously studied.

Thermostable SERT–Fab complex

Wild-type human SERT[22] is unstable in detergent micelles and refractory to crystallization. We thus screened a panel of SERT mutants for enhanced thermostability using a high-throughput ligand binding assay[23], and by fluorescence-detection size exclusion chromatography[24]. Two thermostabilizing mutations, Ile291Ala and Thr439Ser, were introduced into SERT, yielding the ts2 construct, stable in short-chain detergents. Using transporter protein isolated from baculovirus-transduced mammalian cells[25], together with a recombinant anti-SERT Fab, we obtained small crystals of a ts2–Fab–paroxetine complex that diffracted X-rays to 4.5 Å resolution. To improve crystal order, we included a third thermostabilizing mutation (Tyr110Ala), yielding the ts3 construct, which further improved stability and produced crystals of the Fab complex with either (*S*)-citalopram or paroxetine that diffracted X-rays to 3.15 Å resolution (Extended Data Tables 1 and 2). Whereas the wild-type transporter exhibits serotonin transport with a Michaelis constant (K_m) of $1.9 \pm 0.3\,\mu M$ (mean $\pm$ s.e.m.) and a maximal velocity (V_{max}) of 23 ± 1 pmol min^{-1}, similar to reported values[8], ts2 has a K_m

[1]Vollum Institute, Oregon Health & Science University, Portland, Oregon 97239, USA. [2]Howard Hughes Medical Institute, Oregon Health & Science University, Portland, Oregon 97239, USA.
†Present address: Graduate Group in Biophysics, University of California, San Francisco, San Francisco, California 94158, USA.
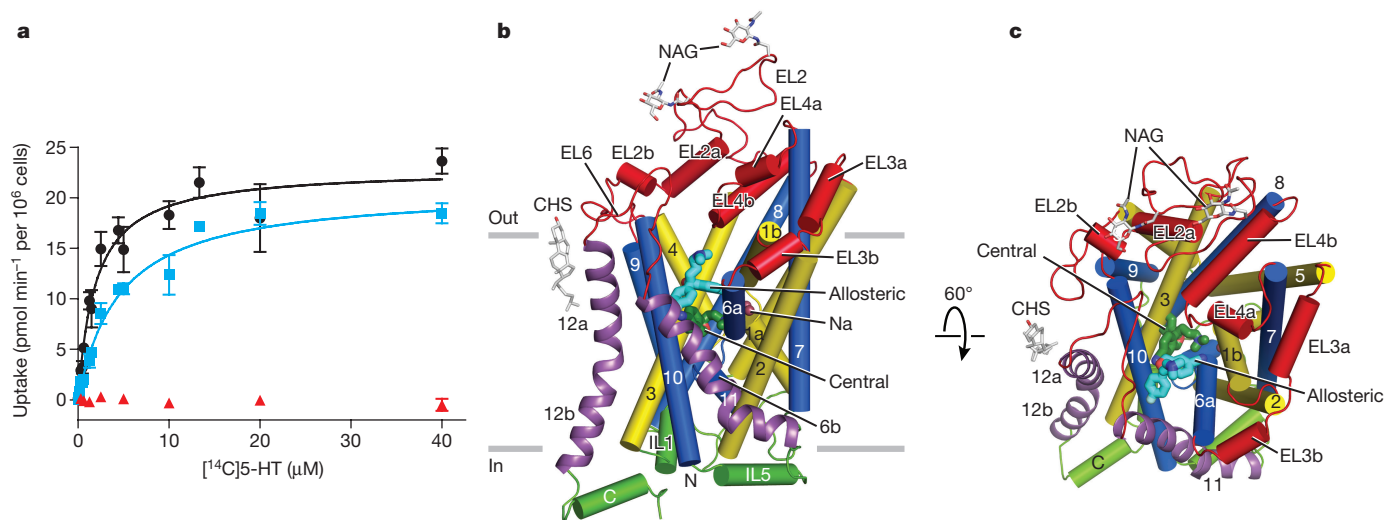
Figure 1 | Function and architecture of the human serotonin transporter. a, Michaelis–Menten plots of serotonin (5-HT) uptake by wild-type (black, circles), ts2 (blue, squares) and ts3 (red, triangles) transporters. Graph depicts an average of three independent experiments, each performed with triplicate measurements (error bars represent s.e.m.). **b**, Structure of SERT viewed parallel to the membrane. The (S)-citalopram molecules at the central and allosteric site are shown as sticks in dark green and cyan, respectively. Sodium ions are shown as spheres in salmon. Cholesteryl hemisuccinate (CHS) and N-acetylglucosamine (NAG) are shown as sticks. **c**, View of SERT from the extracellular side of the membrane.

value of $4.5 \pm 0.6\,\mu M$ and V_{max} value of 21 ± 5 pmol min^{-1} (Fig. 1a). No detectable transport activity was found for ts3.

Architecture of human SERT

The structure of human SERT bound to (S)-citalopram or paroxetine exhibits an outward-open conformation with the antidepressant drug bound to the central site, halfway across the membrane and wedged into a cavity made up of residues from TM1, TM3, TM6, TM8 and TM10 (Fig. 1b, c). A second (S)-citalopram molecule was found in the allosteric site, within the extracellular vestibule of the (S)-citalopram cocrystal structure, approximately 13 Å from the central site. Akin to dDAT and LeuT, SERT has 12 transmembrane-spanning helices with TM1–TM5 and TM6–TM10 related by a pseudo-two-fold axis[14,16,20,21] (Extended Data Fig. 1). The ts2 and ts3 transporters superimpose well (Extended Data Table 3), demonstrating that the additional mutation of the ts3 construct does not substantially perturb the functionally active ts2 transporter structure (Extended Data Fig. 2a). TM1 and TM6 adopt short regions of non-helical conformation as they skirt the central ligand site and contribute residues that bind inhibitors as well as coordinate Na$^+$ and Cl$^-$ ions. The conformations of TM1 and TM6 are incompatible with the formation of an occluded state, suggesting that the antidepressant molecules have locked the transporter in an outward-open conformation, similar to the inhibitor-bound outward-open conformations of dDAT and LeuT[14,16,19,21,26] (Extended Data Table 3).

The extracellular surface of SERT is largely composed of extracellular loop (EL) 2, EL4 and EL6, with EL2 'combed-over' the extracellular surface and providing 3,376 Å^2 of solvent-accessible surface area. A conserved disulfide bridge is formed between Cys200 and Cys209 in EL2 (ref. 27). EL2 is predicted to contain two N-linked glycosylation sites, Asn208 and Asn217 (ref. 28), and electron density for a N-acetylglucosamine moiety was found linked to Asn208; weak density was also found near Asn217. Similar to dDAT, the intracellular surface of the transporter is capped by intracellular loop (IL) 1, IL5 and the carboxy-terminal helix. Unlike LeuT, yet reminiscent of dDAT, TM12 has a pronounced kink halfway across the membrane. There is a cholesterol hemisuccinate (CHS) molecule bound near TM12a.

The crystal lattice packing between two SERT molecules occurs at the kink in TM12, which also overlaps with a two-fold axis of crystallographic symmetry (Extended Data Fig. 2c), thus generating an apparent SERT 'dimer'. Experiments suggest that SERT is an oligomer

in the membrane[29]. However, in detergent SERT is a monomer and we suggest that the SERT 'dimer' observed in this crystal form is unlikely to exist in a membrane bilayer because the predicted membrane-spanning regions of each protomer are not aligned with one another. Because the electron density for the Fab constant domain was poor, we also solved the structure of the Fab at 1.6 Å resolution to facilitate model building and refinement (Extended Data Fig. 2f and Extended Data Table 1). The Fab binds to a large extracellular surface consisting of EL2 and EL4 in a symmetry-related SERT, and this interface is further stabilized by interactions of EL2–EL2 and Fab–EL2 in the asymmetric unit (Extended Data Fig. 2d, e).

The structure of SERT shows that amino acid changes due to single nucleotide polymorphisms and mutations associated with psychiatric disorders are distributed throughout the structure (Extended Data Fig. 2b). Interestingly, most of the altered residues face solvent or lipid[12], thus rendering their effect on SERT structure and function obscure. Pro339Leu, however, is located in the non-helical region of TM6 neighbouring the ligand-binding site and, not surprisingly, this variant exhibits diminished transport activity. By contrast, other disease-associated mutations and polymorphisms, including mutations at Ile425 in TM8, Lys201Asn in EL2 (ref. 30) and Ser293Phe and Leu362Met in TM5 and TM7 enhance serotonin transport, respectively. Another class of mutations, Phe465Leu in TM9 and Leu550Val in TM11, probably destabilize the transporter or, as in the case of the Lys605Asn substitution in the C-terminal helix, render the transporter insensitive to protein kinase G regulation. With the establishment of SERT structural analysis, together with SERT expression and purification, we can now determine more precisely how these mutations alter the structure and activity of SERT.

Antidepressant bound at the central site

To probe the capacity of the ts2 and ts3 SERT constructs to bind antidepressants, we carried out binding studies using [^{3}H](R/S)-citalopram and [^{3}H]paroxetine (Fig. 2a, b). (R/S)-citalopram binds with dissociation constant (K_d) values of 2.1 ± 0.1, 1.9 ± 0.3 and 2.9 ± 0.5 nM to the wild-type, ts2 and ts3 variants[31], whereas paroxetine exhibits K_d values of 0.08 ± 0.03, 0.17 ± 0.03 and 0.10 ± 0.02 nM for wild-type, ts2 and ts3 constructs[31], respectively.

We next investigated the structure of the antidepressant binding site in the paroxetine and (S)-citalopram complexes by dividing the site into subsites A, B and C[15] (Fig. 2c–e). Multi-crystal
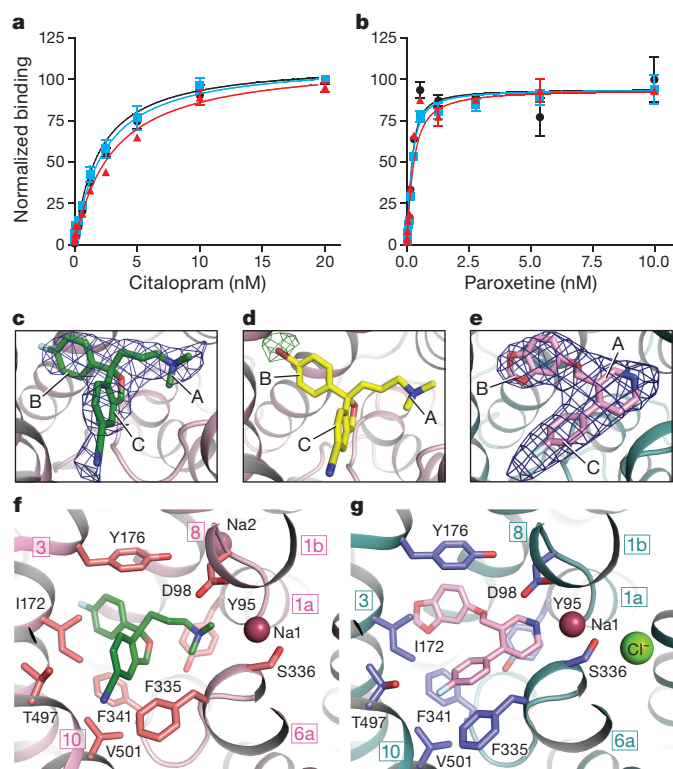
Figure 2 | Antidepressant binding and recognition. a, Graph of [^{3}H](R/S)-citalopram saturation binding to wild-type (black, circles), ts2 (blue, squares) and ts3 (red, triangles) transporters, showing the average of two independent experiments, each performed in triplicate (error bars represent s.e.m.). **b**, Plot of a [^{3}H]paroxetine saturation binding from a representative experiment (error bars represent s.e.m. from triplicate measurements). **c**, $F_o − F_c$ omit (S)-citalopram electron density (blue mesh), contoured at 3σ. The approximate positions of subsites A, B and C are shown. **d**, Anomalous difference electron density (green mesh), derived from Br-citalopram (yellow sticks) bound to the central site is shown (8.0σ contour level). **e**, $F_o − F_c$ omit electron density for paroxetine, contoured at 3σ. **f**, Interactions of (S)-citalopram (dark green) in the central binding site. **g**, Interactions of paroxetine (pink) with residues in the central binding site.

averaging of three (S)-citalopram data sets resulted in electron density maps that supported placement of the cyanophtalane group in subsite C and the fluorophenyl in subsite B, in agreement with detailed mutagenesis and ligand-binding studies[32] (Fig. 2c). Nevertheless, because of the limited resolution of the diffraction data, we wanted to ensure that we had positioned (S)-citalopram correctly. To do this, we crystallized SERT with a bromine derivative of citalopram, (R/S)-1-[3-(dimethylamino) propyl]-1-(4-bromophenyl)-1,3-dihydroisobenzofuran-5-carbonitrile, in which the 4-fluoro group is replaced with a bromine atom (Br-citalopram). Upon analysis of the resulting anomalous difference Fourier map, we found a strong anomalous signal (>9σ) in subsite B, corresponding to the predicted position of the bromine atom of the Br-citalopram derivative and, by extension, the fluorine atom of (S)-citalopram (Fig. 2d). These data are consistent with the fluorophenyl group of (S)-citalopram occupying subsite B. The non-therapeutic R-enantiomer of citalopram has markedly weaker affinity for SERT, perhaps because the aromatic substituents swap subsites, relative to the S-enantiomer[33]. Inspection of $F_o − F_c$ omit electron density maps allowed placement of paroxetine in the central binding site with the benzodioxol and fluorophenyl groups in subsites B and C (Fig. 2e). It is noteworthy that the chemically equivalent fluorophenyl groups of (S)-citalopram and paroxetine are positioned in different subsites.

The amine groups of (S)-citalopram and paroxetine occupy subsite A and interact with the carboxylate of the conserved Asp98 (ref. 34) at a distance of 4.1 and 3.1 Å (Fig. 2f, g), perhaps explaining, in part, why paroxetine has a higher affinity for SERT in comparison to (S)-citalopram. Tyr95 localizes 4.2 and 5.3 Å beneath the amine groups of (S)-citalopram and paroxetine, forming a cation–π interaction crucial for citalopram and mazindol potency[35]. Tyr95 may also form a hydrogen bond with the oxygen of (S)-citalopram. Ser336 partners in an interaction network with ligands and ions by participating in Na$^+$ and Cl$^−$ coordination, ions that are essential for ligand binding and substrate transport[36–38].

Subsite B is particularly important for high-affinity antidepressant interaction as evidenced by mutations that influence citalopram binding[32,39]. Tyr176 engages in hydrophobic interactions with the fluorophenyl and benzodioxol groups of (S)-citalopram and paroxetine while also hydrogen bonding with Asp98. Ile172 and Phe341 define a non-polar ridge that cradles the hydrophobic groups of the drugs, and inhibitor binding is weakened upon mutation of these residues[32,40]. Phe341 in SERT, which is equivalent to Phe325 in dDAT, has swung 'downward' by nearly 40° and forms an aromatic interaction with the 'face' of the cyanophtalane of (S)-citalopram and with the 'edge' of the fluorophenyl group of paroxetine (Extended Data Fig. 3a, b). Ser439, Leu443, Ala169 and Ala173 define a cavity that is more hydrophobic in SERT in comparison to the equivalent cavity in dDAT, and into which the fluorine and dioxol ring groups of (S)-citalopram and paroxetine are inserted (Extended Data Fig. 3c). The fluorophenyl group of (S)-citalopram is positioned 1.5 Å deeper into this space compared with the benzodioxol of paroxetine (Extended Data Fig. 3b).

The fluorophenyl group of paroxetine stacks parallel to the ring of Phe335 in subsite C. By contrast, for (S)-citalopram, the cyanophtalane forms an edge-to-face aromatic interaction. Phe335 defines the extracellular gate, and TM1 and TM6 are markedly different when comparing SERT to dDAT bound to a substrate analogue[19] (Extended Data Table 3), showing that (S)-citalopram and paroxetine 'prop' TM6a in an outward-open conformation. Val501 and Thr497 form a mixed non-polar/polar surface into which the fluoro and cyano groups of paroxetine and (S)-citalopram are found. In the case of (S)-citalopram, the cyano group is inserted 2.1 Å further into subsite C, and the hydroxyl group of Thr497 is positioned 1.7 Å away from its position in the paroxetine state (Extended Data Fig. 3b). In accord with the SERT–citalopram X-ray structure, a modest increase in citalopram affinity is observed for the Thr497Ala mutant[39], which would allow additional space for the cyano group.

Ion–binding sites

Na$^+$ and Cl$^−$ ions, which are essential for substrate transport and SSRI binding[41], could be identified with electron densities >3σ in $F_o − F_c$ 'omit' maps (Extended Data Fig. 4), at positions similar to those found in dDAT (Extended Data Table 4). The Na1 site is made up of residues contributed from TM1, TM6 and TM7 and the ion is coordinated by Ala96, Asn101, Ser336 and Asn368. Whereas Na1 is coordinated, in part, by a water molecule in dDAT, which in turn is hydrogen-bonded to Asp46, in SERT there is not sufficient density to place water at a similar position. The chloride ion is coordinated by Tyr121, Gln332, Ser336 and Ser372 from TM2, TM6 and TM7 with a mean coordination distance of 3.1 Å. Strong density for Na2 could be seen in the (S)-citalopram structure with the ion coordinated by Gly94, Val97, Leu434, Asp437 and Ser438 from TM1 and TM8. Placing ions in the omit densities led to a loss in $F_o − F_c$ density and the B-values of the ions match the values of surrounding residues. The mean coordination distance (2.4 Å) corresponds to known coordinate distances for sodium[42]. Only weak density for Na2 could be seen in the paroxetine structure, while in the (S)-citalopram complex the density for Cl$^−$ was weak, perhaps reflecting the overall weaker density in these regions rather than a difference in occupancy.
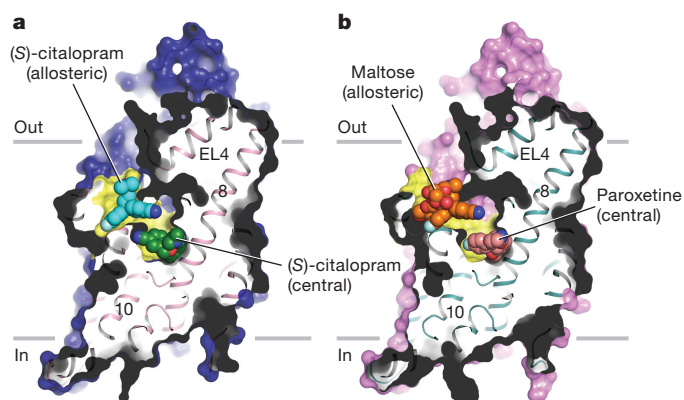
Figure 3 | Allosteric site. a, Sagittal slice through a surface representation of the (S)-citalopram-bound transporter. (S)-citalopram molecules bound to the allosteric (cyan) and central (green) sites are shown as spheres. **b**, A maltose head group (orange), derived from a detergent molecule and bound to the allosteric site, and paroxetine (pink), bound to the central site, are shown as spheres.

Figure 4 | Structural features of the allosteric site. a, Dissociation of $[^3H](R/S)$-citalopram in the presence of buffer containing $100\,\mu M$ (S)-citalopram (circles) or without ligand (squares). A representative experiment is shown (error bars represent s.e.m. from triplicate measurements). **b**, Allosteric site bound with (S)-citalopram (cyan). Residues in close proximity to (S)-citalopram are shown as sticks. A few atoms of (S)-citalopram at the central site (green sticks) are visible 'below' the (S)-citalopram molecule bound to the allosteric site. $F_o - F_c$ omit density of (S)-citalopram (blue mesh) in the allosteric site is shown (1.5σ contour level). **c**, Anomalous difference electron density (green mesh), derived from a Br-citalopram (yellow sticks) diffraction data set, is contoured at 5σ. **d**, Alignment of the allosteric site of the paroxetine (blue) and (S)-citalopram-bound (pink) structures. Maltose is in orange sticks. Superposition was performed over all Cα atoms of the transporter.

Extracellular and intracellular gates

The SERT–SSRI complexes adopt an outward-open conformation that exposes the cone-shaped extracellular vestibule to aqueous solution, providing a pathway for substrates, inhibitors and ions to reach the central binding site, approximately halfway across the membrane bilayer. As in LeuT, the extracellular vestibule contains residues that form the extracellular gate, and is lined by TM1b and TM6a, as well as by extracellular regions of TM3, TM8, TM10 and TM11, together with EL6 and the 'tip' of EL4. The mixed polar and non-polar character of the extracellular vestibule provides low affinity binding sites for small molecules, similar to LeuT, and in SERT we find electron density attributed to a second (S)-citalopram molecule in the (S)-citalopram cocrystal structure and a maltose detergent head group in the paroxetine complex within the extracellular vestibule[14,43–45] (Fig. 3a, b).

At the base of the vestibule is the extracellular gate, and near the cytoplasmic face of SERT is the intracellular gate (Extended Data Fig. 5a, b). In SERT, Tyr176 and Phe335 define the lower portion of the extracellular gate and are separated by a distance of 10 Å, thus providing open access to the extracellular vestibule. In comparison to the extracellular gate of dDAT, the equivalent region in SERT exhibits notable structural changes: Tyr176 and Asp98 are separated by 4.0 Å and TM10 is closer to TM1b, bringing Glu494 and Arg104 within 4.8 Å, and thus the central site can only be accessed through the extracellular vestibule. The intracellular gate of SERT is closed, similar to the outward facing conformations of dDAT and LeuT, thus precluding direct access from the central ligand binding site to the intracellular solution (Fig. 3 and Extended Data Fig. 5b).

Allosteric site

To determine whether the off-rate of inhibitor from the central site is modulated by a ligand binding to an allosteric site in the ts3 construct, we measured the dissociation of $[^3H](R/S)$-citalopram from the central site in the presence of saturating concentrations of cold (S)-citalopram. As shown in previous studies, micromolar concentrations of (S)-citalopram, serotonin and other ligands slow dissociation from the central site[10,11]. For ts3, $100\,\mu M$ (S)-citalopram decreased the first-order rate of $[^3H](R/S)$-citalopram dissociation by nearly tenfold compared to buffer alone (0.0032 ± 0.0007 versus $0.025 \pm 0.002\,min^{-1}$) (Fig. 4a), with the wild-type and ts2 transporters exhibiting similar effects (wild-type: 0.004 ± 0.001 versus $0.035 \pm 0.004\,min^{-1}$; ts2: 0.0028 ± 0.001 versus $0.08 \pm 0.03\,min^{-1}$), thus showing that allosteric modulation of ligand unbinding is intact in the ts2 and t3 constructs.

The allosteric binding site of (S)-citalopram is defined by residues in TM1b, TM6a, TM10 and TM11, and in EL4 and EL6 (Fig. 4b

and Extended Data Fig. 5c) with prominent electron density ($>5\sigma$ in $F_o - F_c$ omit maps) present in this region for crystals soaked with (S)-citalopram. Interestingly, mutagenesis of residues proximal to the allosteric site has been reported to severely alter allosteric potency[46] yet the physiological role of this site is not well established[47]. Residues of the extracellular gate, Glu494 and Arg104, are located 4.1 and 4.8 Å from the aminopropyl group, while Asp328 is 6.8 Å away. Arg104 is also located 3.6 Å from the cyanophtalane ring and probably participates in a cation–π interaction, while the cyano group of the phtalane ring is 3.1 Å from the side-chain amide of Gln332. Ala331 forms a non-polar groove into which the ring system of (S)-citalopram is buttressed. Phe556 is 3.5 Å from the fluorophenyl group and participates in aromatic interactions while a proline repeat (Pro560–Pro561) in EL6 demarcates the upper portion of the allosteric site, 6.6 Å from the fluorophenyl entity.

To confirm the identity of the ligand bound to the allosteric site, we soaked crystals with Br-citalopram. A strong anomalous signal ($>5\sigma$) corresponding to bromine was detected in anomalous difference electron density maps, confirming the position and pose of citalopram in the allosteric site (Fig. 4c). However, there was not sufficient electron density to place the aminopropyl group of Br-citalopram and thus we excluded it from the structure.

In the paroxetine complex, we found electron density for a putative maltose entity, presumably derived from a detergent molecule (Extended Data Fig. 5d) occupying a position in the extracellular vestibule that partially overlaps with (S)-citalopram bound in the allosteric site (Fig. 4d). Upon analysis of the allosteric site of the (S)-citalopram and paroxetine complexes, we note considerable plasticity, presumably owing to the nature of the bound molecule. Relative
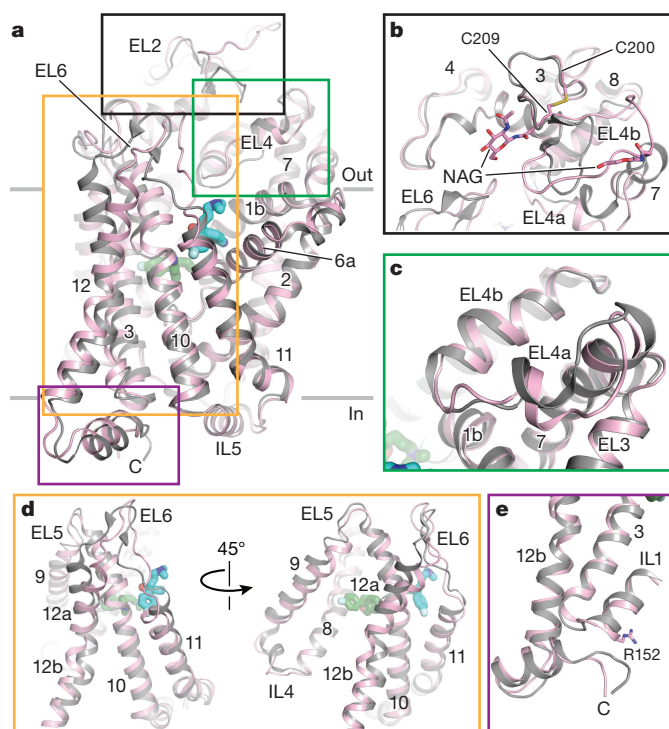
Figure 5 | Comparison of serotonin and dopamine transporters.
a, Overall alignment of SERT (pink) versus dDAT (grey) using TM1–TM12; regions in SERT with structural differences are boxed. (*S*)-citalopram bound to the central (green) and allosteric (cyan) sites shown as sticks. **b**, Close up view of EL2, *N*-acetylglucosamine (NAG; SERT) and the disulfide bridge between Cys200 and Cys209 are shown as sticks. **c**, View of EL4. **d**, Structural differences at the SERT allosteric site showing TM9, TM10, TM11, TM12, EL6 and IL4. **e**, Conformation of the C-terminal helix and IL1. Arg152 of SERT is shown as sticks.

to the (*S*)-citalopram-bound allosteric site, in the paroxetine structure Phe556 moves 'downwards' towards TM6a, to a position underneath the maltose. In addition, Arg104 moves 2 Å further into the allosteric site, while EL6 also moves 1.3 Å towards TM10, with the largest change occurring at Pro561. The malleability of the allosteric site opens the possibility that, depending on the shape and size of the allosteric ligand, occupancy of the allosteric site might not necessarily abrogate transport activity. Indeed, it is conceivable that there could be a spectrum of small molecules that range from inhibiting to enhancing transport activity.

Comparison of the allosteric site of SERT with the equivalent region of dDAT shows how the SERT site is distinct from that of dDAT, even though SERT and dDAT are highly similar in structure within their cores around the central ligand binding site (TM1–TM8; Extended Data Table 3). Indeed, there are marked differences between SERT and dDAT for TM9–TM12 and the extracellular loops (Fig. 5a and Extended Data Table 3). EL2, centrally positioned within the extracellular domain, is longer in SERT than in dDAT and participates in extensive interactions with EL4 and EL6, which together sculpt a portion of the allosteric site (Fig. 5b, c). Moreover, when comparing the amino acid sequences of human SERT, DAT and NET, EL6 displays one of the highest regions of diversity, consistent with the observation that allosteric ligands of SERT do not modulate DAT or NET. Furthermore, EL6 adopts a unique conformation not observed in dDAT because it extends more than 4 Å further towards EL2.

The conformation of TM9–TM12 also defines the allosteric site (Fig. 5d). Comparisons between dDAT and SERT illustrate that in SERT TM9 is shifted towards TM12, perhaps coordinated by contacts via EL5 and TM10, the latter of which contains a short stretch of π-helix near Glu494, a key residue of the extracellular gate. In SERT,
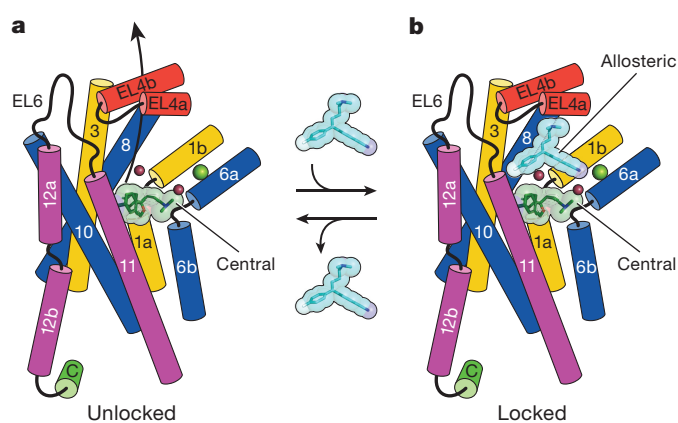
Figure 6 | Allosteric modulation of inhibitor binding. a, The SSRI (*S*)-citalopram (dark green) binds to the central site by wedging between scaffold helices 3, 8 and 10 and core helices 1 and 6. Sodium and chloride ions are shown as salmon and green spheres. **b**, (*S*)-citalopram (cyan) binds to the allosteric site made up of TM1b, TM6a, TM10, TM11, EL4 and EL6. Binding to the allosteric site slows dissociation of inhibitor from the central site.

TM11 extends further into the putative membrane environment in comparison to dDAT, thus providing a larger cavity for allosteric ligands, while TM12a splays inward to buttress TM10 and TM11. Finally, interaction of cholesterol, which is known to modulate transport and ligand binding[48] together with other lipid molecules, may reinforce the conformation of TM12. Indeed, in SERT a CHS molecule stacks against Trp573 in a groove formed by Leu577, Ile576 and Ala580 and the extracellular portion of TM12a (Extended Data Fig. 6b), along with a presumed alkyl chain of a detergent molecule bound in a cavity composed of residues from TM10 and TM12a (Extended Data Fig. 6c).

Intracellular surface and C-terminal hinge
IL5 and the intracellular half of TM11 are highly similar to dDAT, while IL4 is partially unwound due to the insertion of Trp458 (Fig. 5d). The C terminus of SERT mimics dDAT with a similar hinge and helix region (Fig. 5e). Glu615 is thought to form a salt bridge with Arg152 in IL1 (ref. 49), but no side-chain density is present, which makes assignment of C-terminal register not possible. We propose that the disorder of the C terminus is due to dynamic properties, perhaps related to its importance in trafficking[50].

Conclusion
The SERT–SSRI complexes capture the transporter in an inhibitor-bound, outward-open conformation, illustrating how the bulky ligands lodge in the central binding site, preventing substrate binding and transporter isomerization to occluded and inward-open conformations. Extensive interactions throughout the central binding site explain, in large part, the selectivity of SSRIs. The allosteric site is poised 'above' the central site, within the 'walls' of the extracellular vestibule, directly obstructing ligand egress from the central site, thus explaining how allosteric ligands slow the off-rate of inhibitors bound to the central site (Fig. 6). Taken together, the structures of the human serotonin transporter shed fresh insight into antidepressant recognition and the molecular basis for allosteric modulation of inhibitor binding and of transporter activity, thus providing a platform to design small molecules targeting the central and allosteric binding sites.

1. Berger, M., Gray, J. A. & Roth, B. L. The expanded biology of serotonin. *Annu. Rev. Med.* **60,** 355–366 (2009).
2. Rapport, M. M., Green, A. A. & Page, I. H. Serum vasoconstrictor, serotonin; isolation and characterization. *J. Biol. Chem.* **176,** 1243–1251 (1948).
3. Blackburn, K. J., French, P. C. & Merrills, R. J. 5-hydroxytryptamine uptake by rat brain *in vitro. Life Sci.* **6,** 1653–1663 (1967).
4. Carlsson, A., Fuxe, K. & Ungerstedt, U. The effect of imipramine on central 5-hydroxytryptamine neurons. *J. Pharm. Pharmacol.* **20,** 150–151 (1968).
5. Glowinski, J. & Axelrod, J. Inhibition of uptake of tritiated-noradrenaline in the intact rat brain by imipramine and structurally related compounds. *Nature* **204,** 1318–1319 (1964).
6. Hoffman, B. J., Mezey, E. & Brownstein, M. J. Cloning of a serotonin transporter affected by antidepressants. *Science* **254,** 579–580 (1991).
7. Blakely, R. D. *et al.* Cloning and expression of a functional serotonin transporter from rat brain. *Nature* **354,** 66–70 (1991).
8. Kristensen, A. S. *et al.* SLC6 neurotransmitter transporters: structure, function, and regulation. *Pharmacol. Rev.* **63,** 585–640 (2011).
9. Bröer, S. & Gether, U. The solute carrier 6 family of transporters. *Br. J. Pharmacol.* **167,** 256–278 (2012).
10. Wennogle, L. P. & Meyerson, L. R. Serotonin modulates the dissociation of [³H]imipramine from human platelet recognition sites. *Eur. J. Pharmacol.* **86,** 303–307 (1982).
11. Zhong, H. *et al.* An allosteric binding site at the human serotonin transporter mediates the inhibition of escitalopram by R-citalopram: kinetic binding studies with the ALI/VFL-SI/TT mutant. *Neurosci. Lett.* **462,** 207–212 (2009).
12. Hahn, M. K. & Blakely, R. D. The functional impact of SLC6 transporter genetic variation. *Annu. Rev. Pharmacol. Toxicol.* **47,** 401–441 (2007).
13. Andersen, J., Kristensen, A. S., Bang-Andersen, B. & Stromgaard, K. Recent advances in the understanding of the interaction of antidepressant drugs with serotonin and norepinephrine transporters. *Chem. Commun. (Camb.)* 3677–3692 (2009).
14. Singh, S. K., Piscitelli, C. L., Yamashita, A. & Gouaux, E. A competitive inhibitor traps LeuT in an open-to-out conformation. *Science* **322,** 1655–1661 (2008).
15. Wang, H. *et al.* Structural basis for action by diverse antidepressants on biogenic amine transporters. *Nature* **503,** 141–145 (2013).
16. Yamashita, A., Singh, S. K., Kawate, T., Jin, Y. & Gouaux, E. Crystal structure of a bacterial homologue of Na⁺/Cl⁻-dependent neurotransmitter transporters. *Nature* **437,** 215–223 (2005).
17. Singh, S. K. & Pal, A. Biophysical approaches to the study of LeuT, a prokaryotic homolog of neurotransmitter sodium symporters. *Methods Enzymol.* **557,** 167–198 (2015).
18. Kazmier, K. *et al.* Conformational dynamics of ligand-dependent alternating access in LeuT. *Nature Struct. Mol. Biol.* **21,** 472–479 (2014).
19. Wang, K. H., Penmatsa, A. & Gouaux, E. Neurotransmitter and psychostimulant recognition by the dopamine transporter. *Nature* **521,** 322–327 (2015).
20. Penmatsa, A., Wang, K. H. & Gouaux, E. X-ray structures of *Drosophila* dopamine transporter in complex with nisoxetine and reboxetine. *Nature Struct. Mol. Biol.* **22,** 506–508 (2015).
21. Penmatsa, A., Wang, K. H. & Gouaux, E. X-ray structure of dopamine transporter elucidates antidepressant mechanism. *Nature* **503,** 85–90 (2013).
22. Ramamoorthy, S. *et al.* Antidepressant- and cocaine-sensitive human serotonin transporter: molecular cloning, expression, and chromosomal localization. *Proc. Natl Acad. Sci. USA* **90,** 2542–2546 (1993).
23. Green, E. M., Coleman, J. A. & Gouaux, E. Thermostabilization of the human serotonin transporter in an antidepressant-bound conformation. *PLoS ONE* **10,** e0145688 (2015).
24. Kawate, T. & Gouaux, E. Fluorescence-detection size-exclusion chromatography for precrystallization screening of integral membrane proteins. *Structure* **14,** 673–681 (2006).
25. Goehring, A. *et al.* Screening and large-scale expression of membrane proteins in mammalian cells for structural studies. *Nature Protocols* **9,** 2574–2585 (2014).
26. Krishnamurthy, H. & Gouaux, E. X-ray structures of LeuT in substrate-free outward-open and apo inward-open states. *Nature* **481,** 469–474 (2012).
27. Chen, J. G., Liu-Chen, S. & Rudnick, G. External cysteine residues in the serotonin transporter. *Biochemistry* **36,** 1479–1486 (1997).
28. Tate, C. G. & Blakely, R. D. The effect of N-linked glycosylation on activity of the Na⁺- and Cl⁻-dependent serotonin transporter expressed using recombinant baculovirus in insect cells. *J. Biol. Chem.* **269,** 26303–26310 (1994).
29. Kilic, F. & Rudnick, G. Oligomerization of serotonin transporter and its functional consequences. *Proc. Natl Acad. Sci. USA* **97,** 3106–3111 (2000).
30. Rasmussen, T. N., Plenge, P., Bay, T., Egebjerg, J. & Gether, U. A single nucleotide polymorphism in the human serotonin transporter introduces a new site for N-linked glycosylation. *Neuropharmacology* **57,** 287–294 (2009).
31. Owens, M. J., Knight, D. L. & Nemeroff, C. B. Second-generation SSRIs: human monoamine transporter binding profile of escitalopram and R-fluoxetine. *Biol. Psychiatry* **50,** 345–350 (2001).
32. Andersen, J. *et al.* Mutational mapping and modeling of the binding site for (S)-citalopram in the human serotonin transporter. *J. Biol. Chem.* **285,** 2051–2063 (2010).
33. Koldsø, H. *et al.* The two enantiomers of citalopram bind to the human serotonin transporter in reversed orientations. *J. Am. Chem. Soc.* **132,** 1311–1322 (2010).
34. Sørensen, L. *et al.* Interaction of antidepressants with the serotonin and norepinephrine transporters: mutational studies of the S1 substrate binding pocket. *J. Biol. Chem.* **287,** 43694–43707 (2012).
35. Barker, E. L. *et al.* High affinity recognition of serotonin transporter antagonists defined by species-scanning mutagenesis. An aromatic residue in transmembrane domain I dictates species-selective recognition of citalopram and mazindol. *J. Biol. Chem.* **273,** 19459–19468 (1998).
36. Forrest, L. R., Tavoulari, S., Zhang, Y. W., Rudnick, G. & Honig, B. Identification of a chloride ion binding site in Na⁺/Cl⁻-dependent transporters. *Proc. Natl Acad. Sci. USA* **104,** 12761–12766 (2007).
37. Kantcheva, A. K. *et al.* Chloride binding site of neurotransmitter sodium symporters. *Proc. Natl Acad. Sci. USA* **110,** 8489–8494 (2013).
38. Humphreys, C. J., Wall, S. C. & Rudnick, G. Ligand binding to the serotonin transporter: equilibria, kinetics, and ion dependence. *Biochemistry* **33,** 9118–9125 (1994).
39. Andersen, J. *et al.* Molecular determinants for selective recognition of antidepressants in the human serotonin and norepinephrine transporters. *Proc. Natl. Acad. Sci. USA* **108,** 12137–12142 (2011).
40. Henry, L. K. *et al.* Tyr-95 and Ile-172 in transmembrane segments 1 and 3 of human serotonin transporters interact to establish high affinity recognition of antidepressants. *J. Biol. Chem.* **281,** 2012–2023 (2006).
41. Tavoulari, S., Forrest, L. R. & Rudnick, G. Fluoxetine (Prozac) binding to serotonin transporter is modulated by chloride and conformational changes. *J. Neurosci.* **29,** 9635–9643 (2009).
42. Zheng, H., Chruszcz, M., Lasota, P., Lebioda, L. & Minor, W. Data mining of metal ion environments present in protein structures. *J. Inorg. Biochem.* **102,** 1765–1776 (2008).
43. Singh, S. K., Yamashita, A. & Gouaux, E. Antidepressant binding site in a bacterial homologue of neurotransmitter transporters. *Nature* **448,** 952–956 (2007).
44. Zhou, Z. *et al.* LeuT-desipramine structure reveals how antidepressants block neurotransmitter reuptake. *Science* **317,** 1390–1393 (2007).
45. Zhou, Z. *et al.* Antidepressant specificity of serotonin transporter suggested by three LeuT-SSRI structures. *Nature Struct. Mol. Biol.* **16,** 652–657 (2009).
46. Plenge, P. *et al.* Steric hindrance mutagenesis in the conserved extracellular vestibule impedes allosteric binding of antidepressants to the serotonin transporter. *J. Biol. Chem.* **287,** 39316–39326 (2012).
47. Jacobsen, J. P. *et al.* The interaction of escitalopram and R-citalopram at the human serotonin transporter investigated in the mouse. *Psychopharmacology (Berl.)* **231,** 4527–4540 (2014).
48. Scanlon, S. M., Williams, D. C. & Schloss, P. Membrane cholesterol modulates serotonin transporter activity. *Biochemistry* **40,** 10507–10513 (2001).
49. Koban, F. *et al.* A salt bridge linking the first intracellular loop with the C terminus facilitates the folding of the serotonin transporter. *J. Biol. Chem.* **290,** 13263–13278 (2015).
50. Sucic, S. *et al.* Switching the clientele: a lysine residing in the C terminus of the serotonin transporter specifies its preference for the coat protein complex II component SEC24C. *J. Biol. Chem.* **288,** 5330–5341 (2013).

Author Contributions J.A.C., E.M.G. and E.G. designed the project. E.M.G. and J.A.C. developed thermostable constructs for crystallization. J.A.C. performed protein purification, crystallography and biochemical analysis. J.A.C., E.M.G. and E.G. wrote the manuscript.